IEIE Transactions on Smart Processing and Computing, vol. 3, no. 1, February 2014
http://dx.doi.org/10.5573/IEIESPC.2014.3.1.10

Measurement Coding for Compressive Sensing of Color Images

Khanh Quoc Dinh, Chien Van Trinh, Viet Anh Nguyen, Younghyeon Park, and Byeungwoo Jeon

College of Information and Communication Engineering, Sungkyunkwan University / Suwon, Korea
{dqkhanh, trinhchien, vietanh, neversky, bjeon}@skku.edu

***** Corresponding Author: Byeungwoo Jeon

Received October 20, 2013; Revised October 31, 2013; Accepted November 15, 2013; Published February 28, 2014

** Regular Paper*

***Abstract*:** From the perspective of reducing the sampling cost of color images at high resolution, block-based compressive sensing (CS) has attracted considerable attention as a promising alternative to conventional Nyquist/Shannon sampling. On the other hand, for storing/transmitting applications, CS requires a very efficient way of representing the measurement data in terms of data volume. This paper addresses this problem by developing a measurement-coding method with the proposed customized Huffman coding. In addition, by noting the difference in visual importance between the luma and chroma channels, this paper proposes measurement coding in YCbCr space rather than in conventional RGB color space for better rate allocation. Furthermore, as the proper use of the image property in pursuing smoothness improves the CS recovery, this paper proposes the integration of a low pass filter to the CS recovery of color images, which is the block-based ℓ_{20} -norm minimization. The proposed coding scheme shows considerable gain compared to conventional measurement coding.

***Keywords*:** Compressive sensing, Color image, Measurement coding, Color space conversion

1. Introduction

The high cost of conventional sampling using the Nyquist/Shannon rate [1, 2] for high resolution images has highlighted the need for an alternative sampling scheme. Compressive sensing (CS) [3-6] is one such possibility. For a length-N image vector x (i.e., with N pixels), CS acquires only M measurements, which is formed into a measurement vector y through a linear projection in Eq. (1):

$$y = \Phi x, \tag{1}$$

where Φ is called a measurement matrix, which determines the linear projection of signal x to its measurement vector y. For the recovery of the vector x, the measurement matrix Φ needs to satisfy certain conditions, such as the restricted isometry property [4]. The ratio of $r = M / N$, which is commonly called the subrate or measurement rate, shows how effective the CS scheme is in terms of the sensing cost compared to the conventional Nyquist/Shannon rate.

The measurement matrix Φ has $M \times N$ elements, whose size becomes tremendous in the case of high-resolution images. If sensing is achieved at a frame-basis, N refers to the number of all pixels of the three channels in a picture. As an example of 512×512 color images with 3 color channels at r = 0.5, the size of the measurement matrix is $0.5 \times 3 \times 512 \times 512 = 393216$. Even under the typical practice of processing each channel separately, this size is still quite high. Therefore, instead of frame-based sensing, block-based sensing per channel is a more practical approach [7-10]. Each channel of an image is divided into multiple blocks with a size of $B \times B$. The blocks in each channel are sensed with a small measurement matrix Φ_B with a size $M \times N$, where $N = B \times B$ and $M = r \times N$. In this way, the size requirement of the measurement matrix decreases considerably, which can be stored more easily at the sensing part.

In addition to the size issue of the measurement matrix, the measurement data needs to be stored or transmitted,

which raises a new problem of how to encode those measurements efficiently, and is called measurement coding (MC). For grayscale images, some studies based on the DPCM concept [11-13] have already shown their coding efficiency that under an appropriate configuration (quantization step, subrate, and measurement matrix selections), their coding performance can be comparable to conventional JPEG compression. Motivated by these studies, this paper examined a measurement data-encoding method for color images using the DPCM scheme.

To make the MC more practical, the MC should equip itself with an entropy coding scheme to represent the residual measurements efficiently using the minimum number of bits. In this sense, similar to JPEG [14, 15], this study utilized the Huffman coding with a CS-friendly Huffman table synchronization between the encoder and decoder. By noting that the residual measurements obtained by applying DPCM to the measurement data follow the Laplacian distribution [12], this study developed a method that can easily generate a replica of the Huffman table at the decoder upon receiving only the Laplacian parameters (i.e., mean and variance).

Most imaging devices acquire data in RGB space. Therefore, the CS measurements of the color signal are also likely to be from RGB space. The YCbCr space treats the luma (Y) channel differently from the chroma (Cb and Cr) channels [16]. More coding error is bearable in the chroma channels than in the luma channel, and it is exploited widely in conventional image/video coding. For example, JPEG encodes the color image with different quantization tables for the luma and chroma channels [14]. Another example is color-subsampling, which is more commonly referred to as the 4:2:2 or 4:2:0 format [16]. Therefore, this paper proposes sensing in RGB space to support wider acquisition applications but encode the measurements in YCbCr space to achieve better coding performance.

This paper is organized as follows. Section 2 briefly presents the background on the conventional block-based CS of color images and MC for grayscale images, and then delivers the proposed MC for compressive sensed color images with color conversion in the measurement domain from RGB to YCbCr space. Section 3 explains the proposed improved CS recovery. Sections 4 and 5 report the experimental results and conclusion respectively.

2. Proposed measurement coding for color images

Owing to the large size of (color) images, it is normally desirable to sense images in a block-based manner, in which each color channel is first divided into multiple non-overlapping blocks of a size $B \times B$, and the blocks are sensed independently by the small sized measurement matrix Φ_B [7-10]. Equivalently, the k^{th} block $\left[\left(x_R^k\right)^T \quad \left(x_G^k\right)^T \quad \left(x_B^k\right)^T\right]^T$ of a color image x is sensed as:

$$\begin{bmatrix} y_R^k \\ y_G^k \\ y_B^k \end{bmatrix} = \begin{bmatrix} \Phi_B & & \\ & \Phi_B & \\ & & \Phi_B \end{bmatrix} \begin{bmatrix} x_R^k \\ x_G^k \\ x_B^k \end{bmatrix} \tag{2}$$

In this way, despite sensing the whole image of three color channels, only one block measurement matrix Φ_B with a small size is stored at the sensing part.

2.1 Improved measurement coding

2.1.1 Directional measurement coding

In a block-based CS of grayscale and color images, the individual measurement data inside a block have no correlation with each other because of the random nature of the measurement matrix. On the other hand, the measurement blocks associated with the same projection (i.e., the same measurement matrix Φ_B) may have a high correlation on a block-by-block basis. This analysis was verified in other studies [11-13] by measuring the correlation using grayscale images, which is normally larger than 0.8. This paper shows that, in RGB color images, the measurements between adjacent blocks associated with the same projection also have a strong correlation. Table 1 lists the average correlation coefficient of the measurement vector y of a block with its upper neighbor y_p calculated using Eq. (3).

$$\rho = E\left\{\frac{\left(y-\bar{y}\right)^T\left(y_p-\bar{y}_p\right)}{\left\|y-\bar{y}\right\|_2\left\|y_p-\bar{y}_p\right\|_2}\right\}, \tag{3}$$

where $\bar{y}$ and $\bar{y}_p$ are the mean values of y and y_p, respectively. The correlation in the measurement domain is larger than 0.8 for all color channels of two test images, Lena and Peppers.

The strong correlation in the measurement domain makes it natural to apply the directional MC [12, 13] to color images to effectively represent its measurements. As shown in Fig. 1, for each color channel, the MC searches for the best predictor (in terms of residual energy) of a block y from its set of neighboring blocks (SNB): west, north, north-west, and north-east blocks. The matching criterion based on the residual energy is:

$$y_{pred} = \min_{\tilde{y}\in SNB}\left\{\left\|y-\tilde{y}\right\|_2\right\} \tag{4}$$

Table 1. Correlation coefficient ρ between the blocks in the measurement domain of RGB images (B = 32, averaged over 5 simulations with 5 Gaussian random measurement matrices)

Sub-rate	Lena			Peppers		
	R	G	B	R	G	B
0.1	0.967	0.873	0.956	0.954	0.804	0.803
0.2	0.974	0.887	0.962	0.959	0.818	0.817
0.3	0.973	0.885	0.960	0.960	0.817	0.816

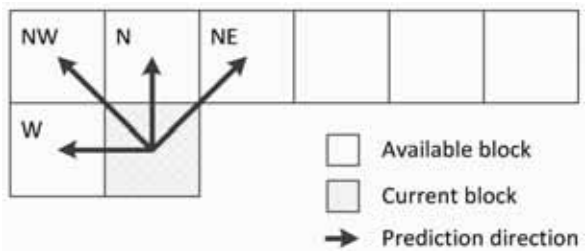

Fig. 1. Directional measurement prediction

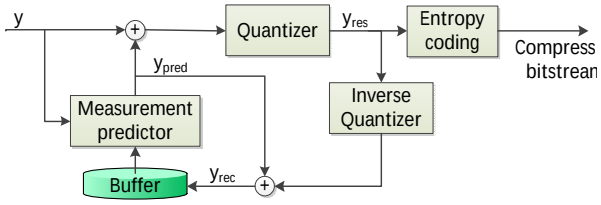

Fig. 2. DPCM scheme of measurement coding.

Note that, the strong correlation among the measurements of the neighboring blocks allows very small residual energy. Hence, the entropy of the residual signal is also expected to be very small. Therefore, for color images, using directional coding [12, 13], the measurement vectors of all blocks can be encoded effectively in RGB space. Fig. 2 shows the directional MC for each color channel, where the residual signal is quantized and subjected to an entropy coding process.

2.1.2 Entropy coding - Huffman coding

In this paper, under the design direction of pursuing low encoding complexity instead of time-consuming arithmetic coding or even context-adaptive arithmetic coding, the Huffman coding was used for its optimality for symbol-by-symbol coding. On the other hand, two issues need to be addressed before Huffman coding can be applied to the measurement data of color images: how to effectively generate a Huffman table, and how to efficiently notify the table to the decoder.

Most residual signals in image/video processing, including the measurement residual y_{res} (residual signal of three color channels obtained by DPCM process), follow Laplacian distribution [12, 26]. Suppose that Y_r is a scalar element of the residual signal vector, y_{res}, obtained from the DPCM process (note that it is quantized before Huffman coding, as shown in Fig. 2), Y_r has a probability distribution of a Laplacian with a mean of μ and a variance of $2/\alpha^2$ as follows:

$$\Pr(Y_r = t) = \frac{\alpha}{2} e^{-\alpha|t-\mu|} \tag{5}$$

As a result, Eq. (5) gives the probability of the event $Y_r = \mu$ as:

$$\Pr(Y_r = \mu) = \frac{\alpha}{2} \tag{6}$$

From Eq. (6), α is approximated by $\alpha = 2 \times f(u)$, where $f(u)$ is the estimated probability of a residual measurement being identical to the mean value of the quantized residual. The probabilities of other values were calculated using Eq. (5). Based on the estimated probabilities, the Huffman table can be constructed. Fig. 3 shows a decent match between the approximated Laplacian distribution and the actual histogram of the quantized measurement residual of the R channel of Lena. This

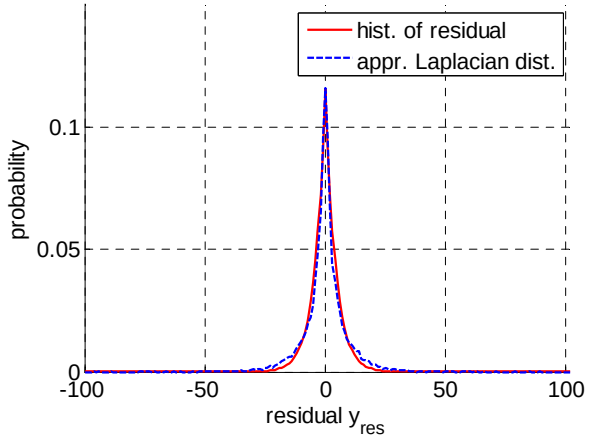

Fig. 3. Histogram of the residual measurement ("hist. of residual") and its approximated Laplacian distribution ("appr. Laplacian dist.") (R-channel of the Lena image, Gaussian random measurement matrix, *r* = 0.3, quantization step of 4).

suggests that the Huffman coding constructed by the estimated probabilities is expected to work well with the directional MC. Furthermore, with only notification of α, μ, and range of residual y_{res}, a decoder can generate an exact replica of the Huffman table used in an encoder for their entropy decoding process.

2.1.3 Proposed RGB-space sensing and YCbCr-space measurement coding

In the previous section, a directional MC scheme was presented for color images in RGB color space. On the other hand, YCbCr space, but not RGB, is known to be more useful in reducing the color redundancy, as is used widely in conventional image/video coding of JPEG and HEVC [14-16]. In those coding frameworks, more error is allowable to the chroma channels (Cb and Cr) to save considerable bitrate while guaranteeing equivalent perceptual quality. To apply that property to the MC of color images, this paper proposes a simple way to convert the measurement from RGB to YCbCr space for encoding without any change in the sensing process.

2.2 Color-space conversion in measurement domain

In the spatial domain, the color-space conversion of the k^{th} block from RGB to YCbCr is calculated easily by a

linear transformation [17-19] as follows:

$$\begin{aligned} x_Y^k &= a_{11}x_R^k + a_{12}x_G^k + a_{13}x_B^k \\ x_{Cb}^k &= x_{128} + a_{21}x_R^k + a_{22}x_G^k + a_{23}x_B^k \\ x_{Cr}^k &= x_{128} + a_{31}x_R^k + a_{32}x_G^k + a_{33}x_B^k \end{aligned}, \quad (7)$$

where x_{128} is a vector with the same size to x_R^k, but has all its values of 128. In addition, a_{11} = 0.299; a_{12} = 0.587; a_{13} = 0.114; a_{21} = -0.168736; a_{22} = -0.331264; a_{23} = a_{31} = 0.5; a_{32} = -0.418688; and a_{33} = -0.081312. Owing to the nature of the linear projections in Eqs. (2) and (7), the measurement vector y_{YCbCr}^k of the k^{th} block in YCbCr space can be calculated from the measurement vector y_{RGB}^k in RGB space as follows:

$$\begin{bmatrix} y_Y^k \\ y_{Cb}^k \\ y_{Cr}^k \end{bmatrix} = \begin{bmatrix} a_{11}y_R^k + a_{12}y_G^k + a_{13}y_B^k \\ y_{128} + a_{21}y_R^k + a_{22}y_G^k + a_{23}y_B^k \\ y_{128} + a_{31}y_R^k + a_{32}y_G^k + a_{33}y_B^k \end{bmatrix}, \quad (8)$$

where y_{128} denotes the measurement vector of x_{128} as $y_{128} = \Phi_B x_{128}$. Therefore, the conversion of color space in the spatial domain is equivalent to the same conversion in the measurement domain. Therefore, the MC can be performed for YCbCr to take advantage of the color decomposition nature of YCbCr. Table 2 lists the spatial correlation of Eq. (3) in the measurement domain of YCbCr space. Obviously, the correlation is also high, resulting in good performance of the directional MC described in the previous section. This paper used the same MC of RGB space in YCbCr space. After reconstructing those measurements in YCbCr space, the recovered YCbCr image, $\bar{x}_{YCbCr}^k$, is converted back to the recovered image in RGB space, $\bar{x}_{RGB}^k$, by:

$$\begin{aligned} \bar{x}_R^k &= \bar{x}_Y^k + b_{13}\left(\bar{x}_{Cr}^k - x_{128}\right) \\ \bar{x}_G^k &= \bar{x}_Y^k + b_{22}\left(\bar{x}_{Cb}^k - x_{128}\right) + b_{23}\left(\bar{x}_{Cr}^k - x_{128}\right) \\ \bar{x}_B^k &= \bar{x}_Y^k + b_{32}\left(\bar{x}_{Cb}^k - x_{128}\right) \end{aligned}, \quad (9)$$

where k is the index of the block being processed, and b_{13} = 1.402; b_{22} = -0.34414; b_{23} = -0.71414; and b_{32} = 1.772.

Table 2. Correlation coefficient ρ between the blocks in the measurement domain of the YCbCr images (B = 32, average over 5 simulations with a Gaussian random measurement matrix).

Sub-rate	Lena			Peppers		
	Y	Cb	Cr	Y	Cb	Cr
0.1	0.934	0.997	0.998	0.900	0.987	0.986
0.2	0.942	0.997	0.998	0.909	0.988	0.988
0.3	0.941	0.997	0.998	0.908	0.988	0.988

2.3 Bit allocation for the YCbCr channels

As discussed in the previous subsection on the different importance of the luma and chroma channels on the human perception of color images, this paper proposes to perform coding differently from channel to channel. That is, luma (i.e., Y) channel should receive the most care because any loss in the Y channel can be recognized easily by the viewers. Therefore, a small quantization step is assigned to MC of the Y channel. For the chroma channels, a large quantization step is used. This has less error in the reconstructed measurement of the Y channel, resulting in good recovery. The large quantization step used for the chroma channels saves bit usage. Note that the relative insensitivity of the human eye to colors makes the relatively larger coding errors in the chroma less perceptible to humans. As a result, the HVS-based tradeoff between the bit amount and recovered quality in YCbCr space provides better rate-distortion performance.

3. Improved recovery of the block-based CS of color images

The block-based CS (BCS) is very important for not only sampling cost reduction but also for effective MC [12]. Accordingly, a corresponding recovery method is in need. For color images, there is an effective recovery method called the smoothed ℓ_{20}-norm minimization [20]. In addition, among the block-based recovery methods for grayscale images, BCS-SPL (Block Compressed Sensing with Smooth Projected Landweber Reconstruction) [8] has high recovery performance arising from its smoothness pursuit. This paper applied the recovery concept of those recoveries [8, 20] to the context of a block-based CS of color images.

Because applying the work reported by Nagesh and Li [20] directly to independent block-by-block recovery may degrade the quality of the recovered image considerably by generating discontinuity in the block boundaries [21-23], the same structure of BCS-SPL [8] was used in the present study to recover all the blocks in parallel with the help of a low pass filter. The low pass filter reduces the discontinuity in the block boundaries. Besides addressing that discontinuity, the smoothness is a very important property of image signals, not only in grayscale but also in all color images. Therefore, the low pass filter also helps in pursuing that important property. Similar to Mun and Fowler [8], a Wiener filter was applied with a window size of 3×3 as a low pass filter at the end of each iteration of the ℓ_{20}-norm minimization [20]. Table 3 lists the improved recovery method for color images step by step. Details of the smoothed ℓ_{20}-norm minimization are reported elsewhere [20].

Finally, in this paper, the proposed MC for color images was composed of four phases: sensing using Eq. (2); color space conversion using Eq. (8); coding and decoding as shown in section 2; recovery in Table 3; and color space conversion using Eq. (9) as shown in the flowchart (Fig. 4).

Table 3. Improved CS recovery for color images with a Wiener filter.

Input: Φ_B, transform matrix Ψ, y, $\sigma_{\min}$, maximum iteration $i_{\max}$, initial x_0
Output: $\bar{x}$
Equivalent matrix: $A = diag(\Phi_B, 3)\, diag(\Psi, 3)$
for all k^{th} block: $s_k = diag(\Psi, 3)\, x_{0;k}$ **end**
Initiate σ
while $\sigma > \sigma_{\min}$ and $k < k_{\max}$ **do**
  for all k^{th} block with its j^{th} element
    1. Calculate $\Delta s_k = \left[s_k(j) \exp\left(-\left\| s_k(j) \right\|_2^2 \right) \right]^T$
    2. Update $s_k^* = s_k - \mu \Delta s_k$
    3. Project $s_k = s_k^* - A^T \left(A^T A \right)^{-1} \left(A s_k^* - s_k \right)$
  end of for
  perform Wiener filter with window [3,3]
  update σ, $i = i + 1$
end of while
for all k^{th} block: $\bar{x}_k = diag(\Psi, 3)^T s_k$ **end**

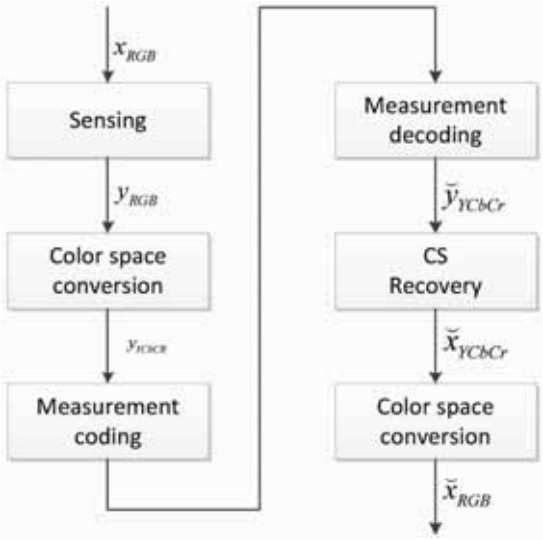

Fig. 4. Flowchart of the propped coding scheme for CS of color images.

4. Experimental results

The proposed methods were verified with four 512×512 color images; Lena, Peppers, Mandrill, and Jet (Fig. 5). The block size of sensing was 32×32, which is a tradeoff of the performance between MC and CS recovery. A uniform quantizer is used in MC with quantization steps of 4 for the RGB channels, and 4/8/8 respectively for the Y, Cb, and Cr channels. The measurement matrix has its entries following an i.i.d. Gaussian random distribution. Owing to the random nature of the measurement matrix, at each configuration of test, 5 simulations were performed and the average of the results was used for a more reliable performance evaluation.

(a) Lena (b) Peppers

(c) Mandrill (d) Jet

Fig. 5. Test images.

Table 4. Three test schemes.

Scheme	Color space for MC	Recovery
Scheme 1	RGB	Block-by-block ℓ_{20}-norm minimization [20] without a Wiener filter
Scheme 2	YCbCr	Same as Scheme 1
Scheme 3		The proposed improved CS recovery in Section 3

As discussed in Section 2, the proposed method of MC with Huffman coding can be used either in the RGB or YCbCr space. Table 4 lists the schemes tested in this study, which are different from each other either by the color space to perform the directional MC (with Huffman coding) or by their recoveries. Because the sensing and coding parts are the same in Schemes 2 and 3, the bit-per-pixel numbers of them are identical.

(a) Coding performance of MC in YCbCr space

Different encoding of the luma (Y) channel from the chroma (Cb and Cr) channels helps save a large number of bits, while degrading the quality of the recovered images only slightly.

The percentage of saved bits was calculated using the following equation:

$$BitSaving = \frac{bpp_{RGB} - bpp_{YCbCr}}{bpp_{RGB}} \times 100\%, \qquad (10)$$

where bpp_{RGB} and bpp_{YCbCr} are the *bpp* (bits per pixel) of MC performed in RGB and YCbCr space, respectively. Note that the *bpp* counts all three color channels together.

Table 5. Rate-distortion performance comparison (bpp vs. PSNR or FSIMc).

(bpp: bit per pixel (all color channels) including all bit overhead; BD-PSNR$^{2-1}$: Bjontegaard differences in PSNR [24] between Schemes 2 and 1 (anchor); the "+" sign means Scheme 2 is better)

subrate	MC in RGB space			MC in YCbCr space					Comparison		
	Scheme 1			bpp (B)	Scheme 2		Scheme 3		Bit Saving (B vs. A) (%)	BD-PSNR$^{2-1}$ [dB]	(C-D) [dB]
	bpp (A)	PSNR	FSIMc		PSNR (C)	FSIMc	PSNR (D)	FSIMc			
Lena											
0.1	1.499	18.867	0.784	0.986	15.862	0.779	23.248	0.887	34.223		7.386
0.2	3.019	26.792	0.927	1.991	26.588	0.926	28.847	0.946	34.051		2.259
0.3	4.518	28.933	0.958	2.977	28.531	0.957	30.307	0.964	34.108	+2.764	1.776
0.4	6.033	30.730	0.974	3.978	30.056	0.973	31.393	0.974	34.063		1.337
avg.	3.767	26.331	0.911	2.483	25.260	0.909	28.449	0.943	34.111		3.190
Peppers											
0.1	1.598	18.230	0.765	1.170	16.466	0.778	23.008	0.888	26.783		6.542
0.2	3.220	26.331	0.913	2.358	26.045	0.911	28.793	0.95	26.770		2.748
0.3	4.817	28.681	0.950	3.526	28.202	0.948	30.274	0.968	26.801	+2.077	2.072
0.4	6.431	30.288	0.968	4.71	29.586	0.967	31.226	0.978	26.761		1.64
avg.	4.017	25.883	0.899	2.941	25.075	0.901	28.325	0.946	26.779		3.251
Mandrill											
0.1	1.682	16.100	0.739	1.194	14.598	0.728	18.661	0.788	29.013		4.063
0.2	3.389	19.403	0.834	2.408	19.362	0.833	20.57	0.855	28.947		1.208
0.3	5.077	20.369	0.877	3.613	20.305	0.876	21.282	0.888	28.836	+1.032	0.977
0.4	6.780	21.422	0.906	4.812	21.324	0.906	21.989	0.911	29.027		0.665
avg.	4.232	19.324	0.839	3.007	18.897	0.834	20.626	0.861	28.956		1.728
Jet											
0.1	1.545	13.939	0.654	0.944	14.302	0.697	21.777	0.834	38.900		7.475
0.2	3.123	25.466	0.876	1.918	25.284	0.875	27.845	0.919	38.585		2.561
0.3	4.669	28.324	0.925	2.853	27.928	0.924	29.756	0.946	38.895	+4.849	1.828
0.4	6.431	30.288	0.968	3.834	29.861	0.953	31.265	0.962	40.383		1.404
avg.	3.942	24.504	0.856	2.387	24.344	0.862	27.661	0.915	39.190		3.317

Table 5 shows that the mean bpp of the Jet at all three test subrates was reduced from 3.942 to 2.387 when YCbCr is used instead of RGB space for MC (i.e., see Schemes 2 and 1). This means 39.190% of the bits were saved. In the case of Peppers, the bit saving was 26.779% (its bpp changes from 4.017 bits to 2.941 bits). Other images have 28.956% (Mandrill) and 34.111% (Lena) bits reduction.

(b) Performance of Huffman coding

The performance of the proposed Huffman coding for MC was evaluated in terms of the difference between the entropy of quantized residual measurement per pixel (denoted by *epp*) and number of bits actually used by Huffman coding per pixel (denoted by *bpp*) for all three color channels. This difference was calculated explicitly in an overhead percentage, *ovhe*, as:

$$ovhe = \frac{bpp - epp}{epp} \times 100\% \qquad (11)$$

The *ovhe* in Table 6 shows that the proposed Huffman coding has at most 3.837% of the rate overhead in the case of Lena with MC in YCbCr space at a subrate of 0.4

Table 6. Bit overhead (%) by Huffman coding.

(a) Measurement coding in RGB space

subrate	Lena			Pepper		
	bpp	epp	ovhe	bpp	epp	ovhe
0.1	1.499	1.479	1.352	1.598	1.592	0.377
0.2	3.019	2.975	1.479	3.220	3.202	0.562
0.3	4.518	4.450	1.528	4.817	4.788	0.606
0.4	6.033	5.941	1.549	6.431	6.393	0.594
avg			1.477			0.535

(b) Measurement coding in YCbCr space

subrate	Lena			Peppers		
	bpp	epp	ovhe	bpp	epp	ovhe
0.1	0.986	0.954	3.354	1.170	1.149	1.828
0.2	1.991	1.919	3.752	2.358	2.311	2.034
0.3	2.977	2.868	3.801	3.526	3.453	2.114
0.4	3.978	3.831	3.837	4.710	4.611	2.147
avg			3.686			2.031

compared to its entropy value.

(c) Reconstruction Performance in YCbCr space

Although many bits can be saved by coding in the YCbCr domain instead of RGB, the PSNR (averaged over all three channels) of the recovered images can decrease. Table 5 shows that on average, for the four test images of Lena, Peppers, Mandrill, and Jet (see the "avg." row of corresponding test images), the degradations (i.e., differences in PSNR between the performance of Scheme 2 and performance of Scheme 1) were 1.071 dB, 0.808 dB, 0.426 dB, and 0.160 dB, respectively.

(d) Rate-Distortion performance of MC in YCbCr space

Regarding both bit saving and PSNR degradation, the BD-PSNR [24] was calculated to evaluate the effectiveness of Scheme 2 over Scheme 1 (anchor) in the overall rate-distortion sense. As shown in Table 5, the BD-PSNR between Schemes 2 and 1 (i.e., BD-PSNR$^{2-1}$) was up to +4.849 dB for the image of the Jet; while still being +1.032 dB for a much detailed image of Mandrill. This shows that Scheme 2 is significantly better than Scheme 1 in terms of the overall rate-distortion performance.

From a quality assessment viewpoint, it is well known that the PSNR is not the best measure that matches with HVS quite well (i.e., in terms of quality that humans actually perceive). Among the many quality-measuring alternatives to PSNR, the feature similarity for color images (FSIMc) [25] showed its superiority in matching with the perceptual sense of viewers. Note that the bit saving of MC in YCbCr space in Scheme 2 arises from the configuration of large quantization steps for the chroma channels of Cb and Cr, which might not play the most significant role in the perceived quality. Therefore, the quality assessment of FSIMc was also measured. Table 5 also shows that despite the large number of saved bits (e.g., 39.190% saved bits in the case of the Jet image), FSIMc does not change much between Schemes 1 and 2. For the Lena image, the FSIMc only decreases from 0.911 (Scheme 1) to 0.909 (Scheme 2). Similarly, Mandrill shows only 0.005 degradation in the FSIMc, whereas for Jet and Peppers, FSIMc even increases by 0.006 and 0.002 from Schemes 1 to 2, respectively.

(e) Performance of the improved recovery

Note that with an embedded Wiener filter, the recovery pursues smoothness, which is a very important property of the image signal (irrespective of RGB or YCbCr spaces). This prior information integrated with a CS recovery method helps improve the quality of the recovered images, particularly for smooth images of Peppers and Jet. In Table 5, the gain of Scheme 3 over Scheme 2 was on average, 3.251 dB for the Peppers image and 3.317 dB for the Jet image. On the other hand, a smaller (average) gain by the improved recovery of 1.728 dB was observed in the case of the detailed image like Mandrill. For Lena, the gain was 3.190 dB using a similar calculation.

At very low subrates, such as 0.1 or 0.2, the conventional recovery method [20] cannot perform well for the following reasons: little information in such few measurements; and those measurements even contain errors (quantization error). For example, at a subrate of 0.1, Nagesh and Li [20] could provide a recovered image quality of 15.8 dB for Lena, and 16.4 dB for Peppers. On the other hand, with the help of a low pass filter, recovery is associated with prior information of the smoothness of images, which is very helpful, where the recovery has less information on the images to be recovered at a low subrate. Therefore, the proposed recovery can provide much better quality, i.e., 23.2 dB and 23.0 dB for Lena and Peppers, which are 7.3 dB and 6.5 dB gains, respectively.

At a high subrate, recovery has much more information on the images to be recovered. Accordingly, prior information on the smoothness is not very important. The proposed recovery provides only 1.3dB and 1.6 dB gains for Lena and Peppers.

(f) Complexity analysis

Here, the time consumption was tested using a measurement encoder and the proposed recovery was assessed using a computer with a configuration of Intel Core i5-2500 3.30GHz, 4GB Ram, and Window 7 32-bit operating system.

Encoding complexity: the encoding time consumed by measurement encoding in RGB space was compared with that in YCbCr space. With a large quantization step for the chroma channels by coding in YCbCr space, the measurement coding consumes less time than that in RGB space, as shown in Table 7(a).

Recovery complexity: The time consumed by the conventional recovery [20] was compared with that of the proposed recovery. With support from prior information of smoothness, the proposed recovery has a greater chance to converge faster despite the additional process of a low pass filter. Accordingly, the time consumption of the proposed recovery is smaller than the recovery [20]. Table 7(b) presents an example of Lena.

5. Conclusion remarks

This paper proposed a measurement coding method equipped with Huffman coding for color images. This

Table 7. Time consumption for Lena, average over 5 simulations.

(a) Encoding complexity

Color space	subrate			
	0.1	0.2	0.3	0.4
RGB	9.9	25.1	35.8	46.7
YCbCr	6.2	14.1	22.1	25.5

(b) Recovery complexity

Recovery	subrate			
	0.1	0.2	0.3	0.4
[20]	164.2	227.7	241.9	252.6
Proposed recovery	154.3	185.9	234.5	227.0

method is novel in sensing in *RGB* space and encoding the measurements in YCbCr space. In this way, although the sensing part can be more widely usable because no changes are needed in the sensing part compared to conventional CS, a more efficient MC is possible because the compressed bit usage can be balanced better considering the visual importance between the luma and chroma channels. For a complete framework, the recovery for CS of the color images with a smoothness pursuit was also improved. The simulation results confirmed the effectiveness and efficiency of the proposed framework.

Acknowledgement

This research was supported by the National Research Foundation of Korea (NRF) grant funded by the Korean government (MSIP) (No. 2011-001-7578).

References

[1] C. E. Shannon, "Communication in the presence of noise", *Proc. Institute of Radio Engineers*, vol. 37(1), pp. 10–21, 1949. Article (CrossRef Link)

[2] H. Nyquist, "Certain topics in telegraph transmission theory," *Trans. AIEE*, vol. 47, pp. 617–644, 1928. Article (CrossRef Link)

[3] D. L. Donoho, "Compressive sensing," *IEEE Trans. on Inform. Theory*, vol. 52(4), pp. 1289-1306, Apr. 2006. Article (CrossRef Link)

[4] E. Candes and T. Tao, "Near-optimal signal recovery from random projections and universal encoding strategies," *IEEE Trans. Inf. Theory*, vol. 52(12), pp. 5406-5425, 2006. Article (CrossRef Link)

[5] H. Lee, S. Park, S. Park, "Introduction to Compressive Sensing," *The magazine of IEEK*, vol. 38(1), pp. 19-30, 2011. Article (CrossRef Link)

[6] Y. M. Cho, "Compressive Sensing - Mathematical Principles and Practical Implications," *The magazine of IEEK*, vol. 38(1), pp. 31-43, 2011. Article (CrossRef Link)

[7] L. Gan, "Block compressed sensing of natural images," *Proc. Intern. Conf. on Digital Signal Process.*, pp. 403-406, UK, 2007. Article (CrossRef Link)

[8] S. Mun and J. E. Fowler, "Block compressed sensing of image using directional transforms," *Proc. IEEE Intern. Conf. on Image Process. (ICIP)*, pp. 3021–3024, 2009. Article (CrossRef Link)

[9] J. Xu, J. Ma, D. Zhang, Y. D. Zhang, and S. Lin, "Improved total variation minimization method for compressive sensing by intra-prediction," *Signal Process.*, vol. 92(11), pp. 2614–2623, 2012. Article (CrossRef Link)

[10] J. Bigot, C. Boyer, and P. Weiss, "An analysis of block sampling strategies in compressed sensing," arXiv:1305.4446 [cs.IT], 2013. Article (CrossRef Link)

[11] S. Mun and J. E. Fowler, "DPCM for quantized block-based compressive sensing of images," *Proc. European Signal Process. Conf.*, pp. 1424-1428, Romania, 2012. Article (CrossRef Link)

[12] K. Q. Dinh, H. J. Shim, and B. Jeon, "Measurement coding for compressive imaing based on structured measurement matrix," *Proc. IEEE Intern. Conf. on Image Process. (ICIP)*, pp. 10-13, 2013. Article (CrossRef Link)

[13] J. Zhang, D. Zhao, and F. Jiang, "Spatially directional predictive coding for block-based compressive sensing of natural images," *Proc. IEEE Intern. Conf. on Image Process. (ICIP)*, pp. 1021-1025, 2013. Article (CrossRef Link)

[14] W. B. Pennebaker and J. L. Mitchell, *JPEG still image data compression standard*, Van Nostrand Reinhold, 1993. Article (CrossRef Link)

[15] S. Shin, H. Go, H. Park, and B. Jeon, "DPCM-Based Image Pre-Analyzer and Quantization Method for Controlling the JPEG File Size," *IEEK for Conf.*, vol. 28(2), pp. 561-564, 2005. Article (CrossRef Link)

[16] G. J. Sullivan, WA. Redmond, J. Ohm, W. Han, and T. Wiegand, "Overview of the High Efficiency Video Coding (HEVC) standard," *IEEE Trans. Circuits and System. for Video Technology*, vol. 22(12), pp. 1649-1668, 2012. Article (CrossRef Link)

[17] K. N. Plataniotis and A. N. Venetsanopoulos, *Color Image Processing and Applications*, Springer, Berlin, 2000. Article (CrossRef Link)

[18] H. Ahn, H. Jeong, J. Ha, K. Kim, and B. Kang, "Improvement Structure of RGB to YCbCr Conversion block of ISP Platform in Mobile Phones," *Proc. Interm. Soc Design Conf.*, pp. 448-451. 2009. Article (CrossRef Link)

[19] A. M.D. Zahangir and H. J. Lee, "A comparative study of different color space for paddy disease segmentation," *The Institute of Electronics Engineers of Korea - Signal Processing*, vol. 3, pp. 90-98, 2001. Article (CrossRef Link)

[20] P. Nagesh and B. Li, "Compressive imaging of color images," *IEEE Int. Conf. Acoust., Speech Signal Process. (ICASSP)*, pp. 1261-1264, 2009. Article (CrossRef Link)

[21] G. Coluccia, D. Valsesia, and E. Magli, "Smoothness-Constrained Image Recovery from Block-based Random Projections," *Proc. IEEE Intern. Workshop on Multimedia Signal Process.*, pp. 129-134, Italia, 2013. Article (CrossRef Link)

[22] H. T. Kung and S. J. Tarsa, "Partitioned compressive sensing with neighbor-weighted decoding," *Proc. IEEE Military Comm. Conf.*, pp. 149-156, USA, 2011. Article (CrossRef Link)

[23] K. Q. Dinh, H. J. Shim, and B. Jeon, "Deblocking filter for artifact reduction in distributed compressive video sensing," *Proc. IEEE Visual Comm. and Image Process.*, pp. 1-5, USA, 2012. Article (CrossRef Link)

[24] G. Bjontegaard, Calculation of average PSNR differences between RD-curves, (VCEG-M33). Article (CrossRef Link)

[25] L. Zhang, L. Zhang, X. Mou, and D. Zhang, "FSIM: a feature similarity index for image quality assessment," *IEEE Trans. Image Process.*, vol. 20(8),

pp. 2378-2386, 2011. Article (CrossRef Link)

[26] C. Brites, J. Ascenso, and F. Pereira, "Studying temporal correlation noise modeling for pixel based Wyner-Ziv video coding" *Proc. of IEEE Int. Conf. on Image Processing*, pp. 273-276, USA, 2006. Article (CrossRef Link)

Khanh Quoc Dinh received his B.S. degree in Electronics and Telecommunications from Hanoi University of Science and Technology, Hanoi, Vietnam, in 2010, a M.S. degree in Electrical and Computer Engineering from Sungkyunkwan University, Suwon, Korea, in 2012. He is currently a Ph.D. candidate in the Digital Media Laboratory at Sungkyunkwan University. His research interests include video compression and compressive sensing.

Chien Van Trinh received his B.S. degree in Electronics and Telecommunications from Hanoi University of Science and Technology, Hanoi, Vietnam, in 2012. He is currently a Master's student in the Digital Media Laboratory at Sungkyunkwan University. His research interest is compressive sensing.

Viet Anh Nguyen received his B.S. degree in Electronics and Telecommunications from Hanoi University of Science and Technology, Hanoi, Vietnam, in 2011, M.S. degree in Electrical and Computer Engineering from Sungkyunkwan University, Suwon, Korea, in 2013. He is currently a Ph.D. candidate in the Digital Media Laboratory at Sungkyunkwan University. His research interests include video compression, and compressive sensing.

Younghyeon Park received his B.S. degree in Electronics Electrical Engineering from Sungkyunkwan University, Suwon, Korea in 2011. He is currently a Ph.D. candidate in the Digital Media Laboratory at Sungkyunkwan University. His research interests include video compression and compressed sensing.

Byeungwoo Jeon received his BS degree in 1985 and an MS degree in 1987 from the Department of Elecronics Engineering, Seoul National University, Seoul, Korea. He received his PhD degree in 1992 from the School of Electrical Engineering at Purdue University, Indiana, United States. From 1993 to 1997 he was in the Signal Processing Laboratory at Samsung Electronics in Korea, where he worked on video compression algorithms, designing digital broadcasting satellite receivers, and other MPEG-related research for multimedia applications. Since September 1997, he has been with the Faculty of the School of Information and Communication Engineering, Sungkyunwan University, Korea, where he is currently a professor. His research interests include multimedia signal processing, video compression, statistical pattern recognition, and remote sensing.